Front. Earth Sci. 2017, 11(2): 427–441
DOI 10.1007/s11707-016-0594-z

RESEARCH ARTICLE

Cenozoic tectonic subsidence in the Southern Continental Margin, South China Sea

Penggao FANG[1], Weiwei DING (✉)[1], Yinxia FANG[1], Zhongxian ZHAO[2], Zhibing FENG[3]

1 The Second Institute of Oceanography, State Oceanic Administration, Hangzhou 310012, China
2 South China Sea Institute of Oceanology, Chinese Academy of Sciences, Guangzhou 510301, China
3 College of Marine Geoscience, Ocean University of China, Qingdao 266100, China

© Higher Education Press and Springer-Verlag Berlin Heidelberg 2016

Abstract We analyzed two recently acquired multi-channel seismic profiles across the Dangerous Grounds and the Reed Bank area in the South China Sea. Reconstruction of the tectonic subsidence shows that the southern continental margin can be divided into three stages with variable subsidence rate. A delay of tectonic subsidence existed in both areas after a break-up, which was likely related to the major mantle convection during seafloor spreading, that was triggered by the secondary mantle convection below the continental margin, in addition to the variation in lithospheric thickness. Meanwhile, the stage with delayed subsidence rate differed along strikes. In the Reed Bank area, this stage is between 32–23.8 Ma, while in the Dangerous Grounds, it was much later (between 19–15.5 Ma). We believe the propagated rifting in the South China Sea dominated the changes of this delayed subsidence rate stage.

Keywords dangerous ground, Reed Bank area, tectonic subsidence, secondary mantle convection, propagated rifting

1 Introduction

The South China Sea (SCS) is one of the largest marginal seas along the western Pacific Margin, and is located in the interacting region of the Pacific, Eurasian, and Indian–Australian plates. It has experienced a complicated geological process, including magma-poor continental rifting, seafloor spreading, the subsequent collision with Borneo to the south, and subduction under the Luzon Arc to the east since the Mesozoic (Taylor and Hayes, 1980,1983; Briais et al, 1993; Zhou et al, 1995; Hutchison, 2004; Cullen, 2010; Li, 2011; Franke, 2013). The continental margin of the SCS constitutes a stretched crust of the continental origin with an area measuring more than 10×10^6 km^2, overlain by numerous Cenozoic sedimentary basins. Previous studies have confirmed that the continental margin of the SCS is a magma-poor passive margin, featured with well-developed detachment systems, depth-dependent stretching, and differences in subsidence, etc. (Ru and Pigott, 1986; Schlüter et al., 1996; Wu et al., 2003; Tong et al., 2009; Ding et al., 2011; Li, 2011) Given these characteristics, the area is not suited for researching continental rifting transition to seafloor spreading.

Although the northern and southern continental margins were connected before opening of the SCS, they preserve remarkable differences in sedimentary faces, environment, and process due to different tectonic subsidence. Thus the analysis on the tectonic subsidence is critical to our understanding of the sedimentary evolution and geodynamics of the Cenozoic extension in the SCS's continental margin. Extensive research has been conducted over the past decades on the tectonic subsidence in different areas of the SCS. Zhao et al. (2011) studied the major tectono-sedimentary stages and their responses to the Cenozoic tectonics by analyzing the changes of the tectonic subsidence in the Dangerous Grounds. On the basis of reconstruction of tectonic subsidence, Ding et al. (2015) explored the development of carbonate platform and the controlling factors. Chen (2014) estimated stretching factors of the Baiyun Sag with multi-stage continental extensional activities by fitting the whole tectonic subsidence history in a self-consistent manner, and explained the mechanism of extreme thick Cenozoic sediment in the study area. Xie et al. (2014) analyzed the Cenozoic tectonic subsidence of the deepwater area in the Pearl River Mouth Basin and constructed maps and histograms of subsidence rate for 18 Cenozoic sequences.

Received October 23, 2015; accepted March 27, 2016

E-mail: wwding@sio.org.cn

All these works play significant roles in increasing our understanding of the sedimentary process and geodynamics of continental margins in SCS. However, few attempts have been made to reconstruct the tectonics subsidence in the same manner or to compare the differences in various sections of the continental margins. Thus, a systematic understanding of the tectono-sedimentary process and dynamic mechanisms during the multi-stage tectonic activities of the SCS is hindered.

In this study, we present a seismo-stratigraphic analysis with two multi-channel seismic profiles across the southern continental margin of the SCS to establish a precise framework with detailed geological interpretation. In addition, we reconstruct the tectonic subsidence history using the empty basin tectonic subsidence method (EBS, Zhao et al., 2013). A better understanding of rifting and opening mechanisms in the SCS relies on comprehensive evaluation of the continental margin, especially the tectonic subsidence, which not only plays an integral role in understanding the extensional processes involved in the formation of rifted margins, but also records the history of the continental break-up and initiation of seafloor spreading. The main goal of this work is to present an overview of the interaction between Cenozoic tectonics and sedimentary features in the SCS, and to determine which model will best explain the featured tectonic subsidence and its relation to tectonic events. The controlling factors and evolution model of the sedimentary process of the southern continental margin during the Cenozoic are also documented.

2 Geological setting

The tectonic evolution of the SCS is dominated by the relative motion and interaction between the Eurasian plate, the Pacific plate and the India Australian plate (Honza, 1995; Lee and Lawver, 1995; Hall, 2002; Honza and Fujioka, 2004; Hall et al., 2008, 2009; Yumul et al., 2008; Aurelio et al., 2012). Due to the subduction of the Pacific plate to the Eurasian plate during the Mesozoic, the entire Southern China margin, including the proto continental margins of the SCS, had been convergent with an Andean-type of volcanic arc (Taylor and Hayes, 1980; Lee and Lawver, 1995; Zhou et al., 1995, 2008; Yao, 1996; Clift and Lin, 2001; Cullen, 2010; Franke et al., 2014). Since the Late Cretaceous, and as a result of subduction slab rollback (Hall, 2002; Li et al., 2007; Zhu et al., 2013; Franke et al., 2014; Li et al., 2014a), the South China continental margin experienced a transition from compression to extension. Episodic rifting with uplifting shoulders and erosion likely began in the proto-continental margin of the SCS. Detailed geological interpretation of seismic profiles suggested that rifting propagated from north to south and from east to west (Li et al., 2012; Ding et al., 2013; Franke et al., 2014; Savva et al., 2014). Two main stages of rifting have been recognized with detailed seismic interpretation (Cullen, 2010; Franke et al., 2014). The former episode predominantly occurred between the Paleocene to Eocene in a NW-SE-oriented extension and is identifiable in nearly all offshore basins. The latter episode took place between the Late Eocene and Early Miocene and was controlled by a NNW-SSE oriented extension. These episodic extensions led to the formation of numerous sedimentary basins with well-developed grabens or half-grabens, such as the Pearl River Mouth Basin and the Qiongdongnan Basin in the north, and the Reed Bank Basin and various basins in the Dangerous Grounds in the south. The accumulation of tensile stress finally led to subsequent seafloor spreading in the SCS.

Scientists have to date based their calculations of the timing of the SCS spreading on the identification of magnetic anomalies. The opening scenario proposed by Taylor and Hayes (1983) and Briais et al. (1993) has been generally accepted, i.e., seafloor spreading occurred from 30 to 16 Ma (anomaly of 11-5C). Since that time, subsequent papers have focused on the spreading mode of the SCS (Barckhausen and Roeser, 2004; Sun et al., 2009; Yeh et al., 2010; Li and Song, 2012; Barckhausen et al., 2014; Franke et al., 2014; Song and Li, 2015), indicating that the Sea experienced two episodes of expansion complicated by a southward ridge jump at nearly 25 Ma and a re-orientation of the spreading geometry from the westward to the southwestward ridge propagation (Taylor and Hayes, 1983; Ru and Pigott, 1986; Briais et al., 1993; Barckhausen and Roeser, 2004; Hayes and Nissen, 2005; Sun et al., 2009; Cullen, 2010; Barckhausen et al., 2014; Franke et al., 2014). This timing was confirmed by deep tow magnetic data (Li et al., 2014b) and IODP Expedition drilling results (Expedition 349 Scientists, 2014). The cessation time is coincident with the collisions between Palawan and Borneo and Mindoro-Central Philippines (Hutchison et al., 2000; Yumul et al., 2003; Clift et al., 2008; Cullen, 2010; Hutchison and Vijayan, 2010), suggesting a causal relationship between the spreading cessation and collision events.

3 Data and methods

3.1 Seismic data

Two multi-channel seismic profiles were interpreted and analyzed. Seismic profile NH973-1 runs across the west of the Spratly Islands in NW-SE trending. Seismic profile NH973-2 lies in the east part of the Reed Bank (Fig. 1). Both profiles were obtained during the "Project 973 Cruise" in 2009 with the Chinese R/V "*Tanbao*". The data were acquired through 480 channels, 6237.5 m-long cable, and were recorded in SEG-D format at a 2 ms sampling interval up to 12 s.

Published dredging data (Kudrass et al., 1986) and data

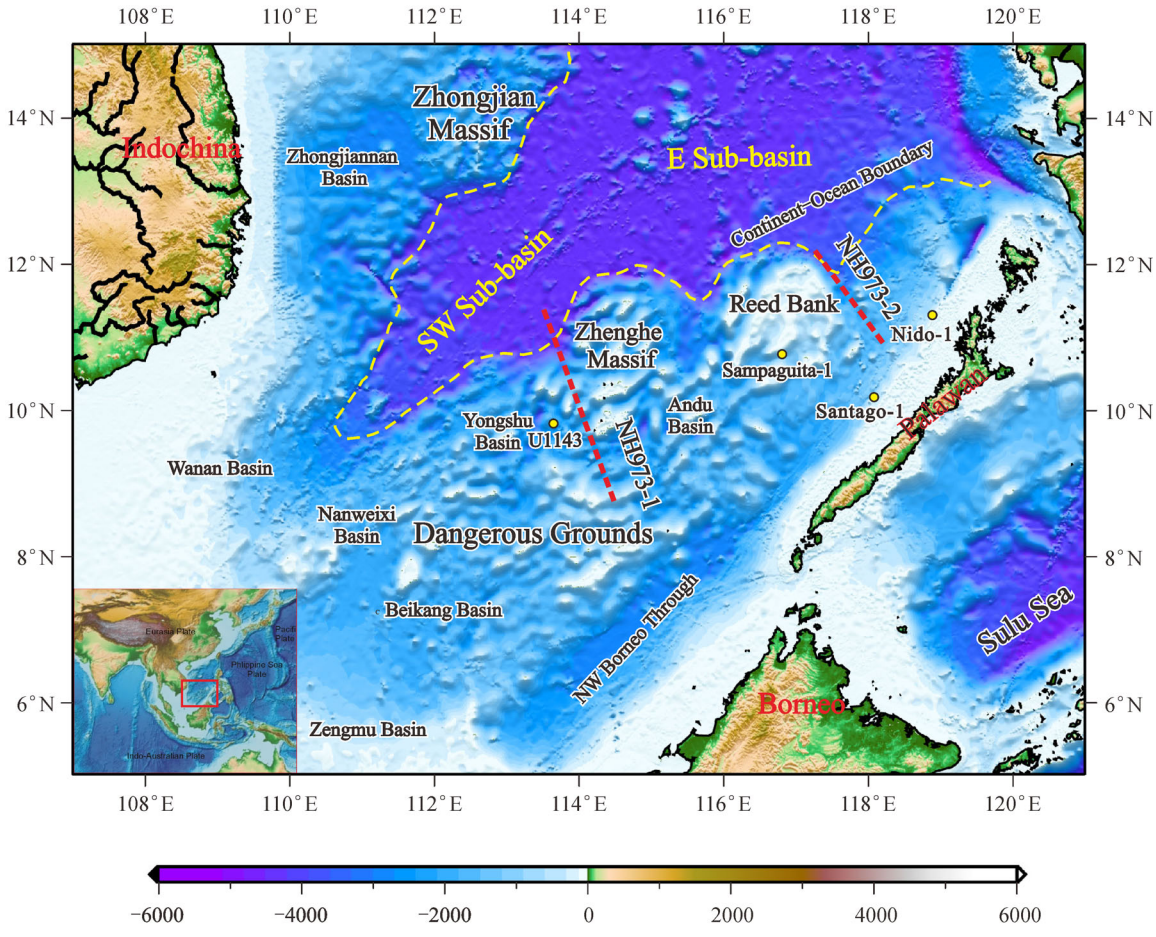

Fig. 1 Morphological features and bathymetry in the southern margin of the South China Sea. Dashed red lines are the seismic profiles used in this study. Yellow circles are the drilling sites. Dashed black lines show the Zhongnan fracture. Dashed yellow lines show the Continental Oceanic Boundary (Franke, 2013).

from limited wells (Sampaguita-1 well in Reed Bank, Nido-1 well and Santiago-1 well offshore Palawan, and ODP Site 1143 in the west of the Dangerous Grounds) were used to calibrate the geological interpretations of seismic sequences carried out on seismic profiles against regional litho-stratigraphic units (see Fig. 1 for locations). In addition, we incorporated published stratigraphic schemes from the study area (Hinz and Schlüter, 1985; Schlüter et al., 1996; Barckhausen and Roeser, 2004; Hutchison, 2004; Yan and Liu., 2004; Clift et al., 2008; Franke et al., 2008; Cullen, 2010; Hutchison and Vijayan, 2010; Ding et al., 2011, 2015; Sun et al., 2011; Yao et al., 2012; Franke, 2013; Savva et al., 2014).

3.2 Identification of sequence boundary (unconformity)

Tectonic subsidence reconstruction is performed by dividing and dating the sequence boundary of the multi-channel seismic profiles. The ages, sedimentary facies, and lithology of the Dangerous Grounds and Reed Bank area are shown in Fig. 2. Geological interpretations of two typical cross sections in the study area are shown in Fig. 3 and Fig. 4. Six sequence boundaries have been identified, including T_g, T_7, T_5, T_4, T_2, and T_0.

T_g is an erosional subsurface boundary, featured by a moderate-to-strong, continuous amplitude that is locally diffractive. It is typically well-defined and corresponds either to the top of tilted blocks or it forms the base of the wedge-shaped syn-rift sedimentary infill. We refer to it as the top of the pre-Cenozoic deposit which is consistent with the onset of continental rifting (Schlüter et al., 1996; Hutchison, 2004; Yan and Liu, 2004; Ding et al., 2013).

T_7 is distinct over both the Dangerous Grounds and Reed Bank areas. It is a regional unconformity that we suggest marking either as an inter-rift status or as the onset of seafloor spreading in the East Sub-basin (ESB) of the SCS, which shows the moderate-to-strong amplitudes and patchy-to-continuous reflectors in the seismic profile. The truncations of the sediments beneath show that it was formed by an erosional event. While an interruption of the extension leading to rifting may not result in erosion, the initiation of seafloor spreading does. We propose that T_7

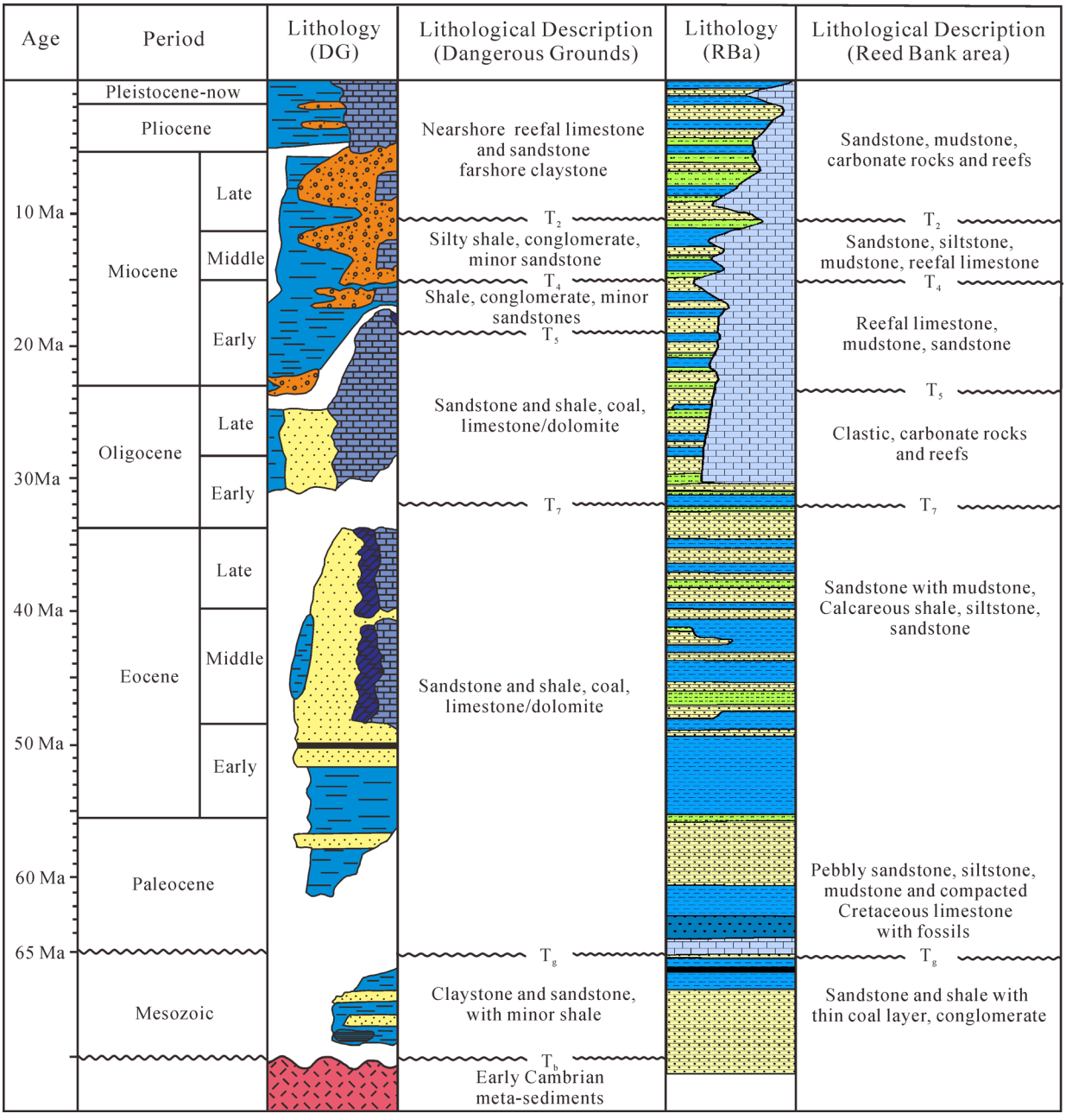

Fig. 2 Seismic stratigraphy and lithology in the Dangerous Grounds and Reed Bank areas.

represents the break-up unconformity (BRU) of the ESB, having an age of about 32 Ma in the eastern sector of the SCS.

T_5 is another major regional unconformity forming both the top of the latest syn-rift sequence in the Reed Bank and Dangerous Grounds areas, as well as the top boundary of the carbonate platform in our study area (Kudrass et al., 1986; Schlüter et al., 1996; Ding et al., 2013, 2015). This sequence boundary is striking in the seismic records, with strong and continuous reflectors, and truncates the sequence beneath. Franke et al. (2014) named it as the end-rifting unconformity (ERU). The age is uncertain since the propagated rifting of the Southwest Sub-basin (SWSB) made the cessation of continental rifting differ from east to west. In the east, ages of 23.8 Ma and between 19–16.5 Ma were determined for the Reed Bank (Yao et al., 2012) and the Dangerous Grounds (Ding et al., 2013) areas, respectively, whereas west of the Dangerous Grounds, an age of 15.5 Ma was assigned (Shipboard Scientific Party, 2000). We agree the age is diachronous, thus we assume an age of 23.8 Ma in the Reed Bank area and 19 Ma east of the Dangerous Grounds. This so-called ERU (Franke et al., 2014) is also a benchmark of the breakup in the SWSB.

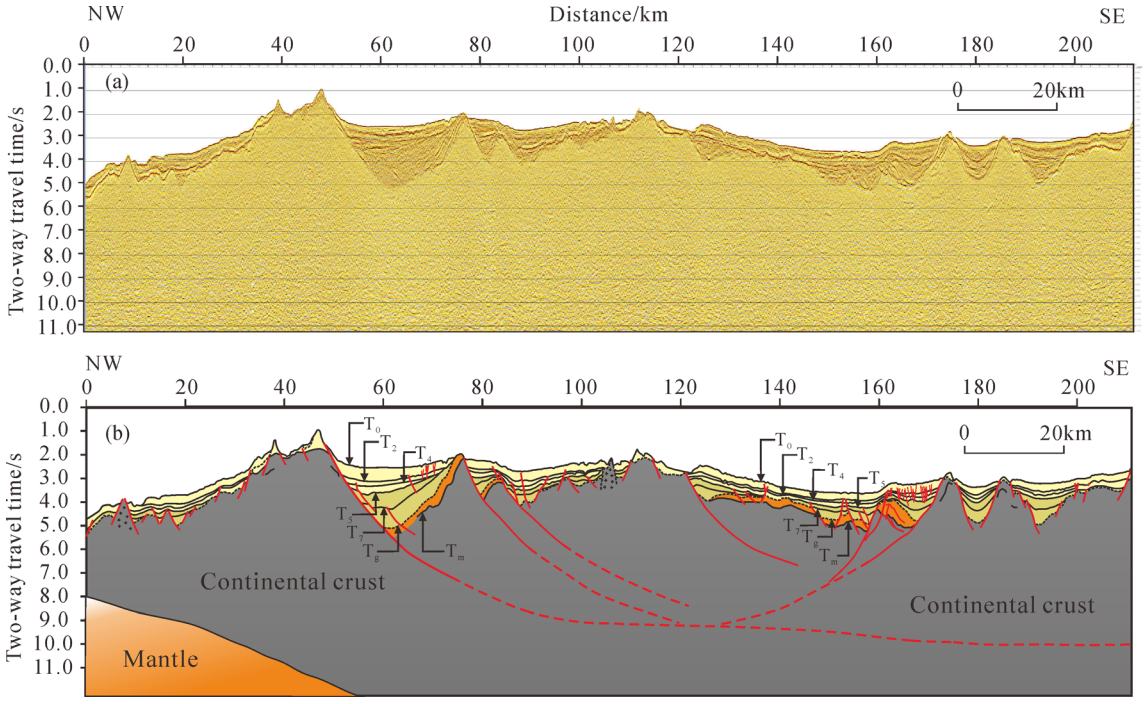

Fig. 3 Geological interpretations of multi-channel seismic profile NH973-1 in the Dangerous Grounds, South China Sea.

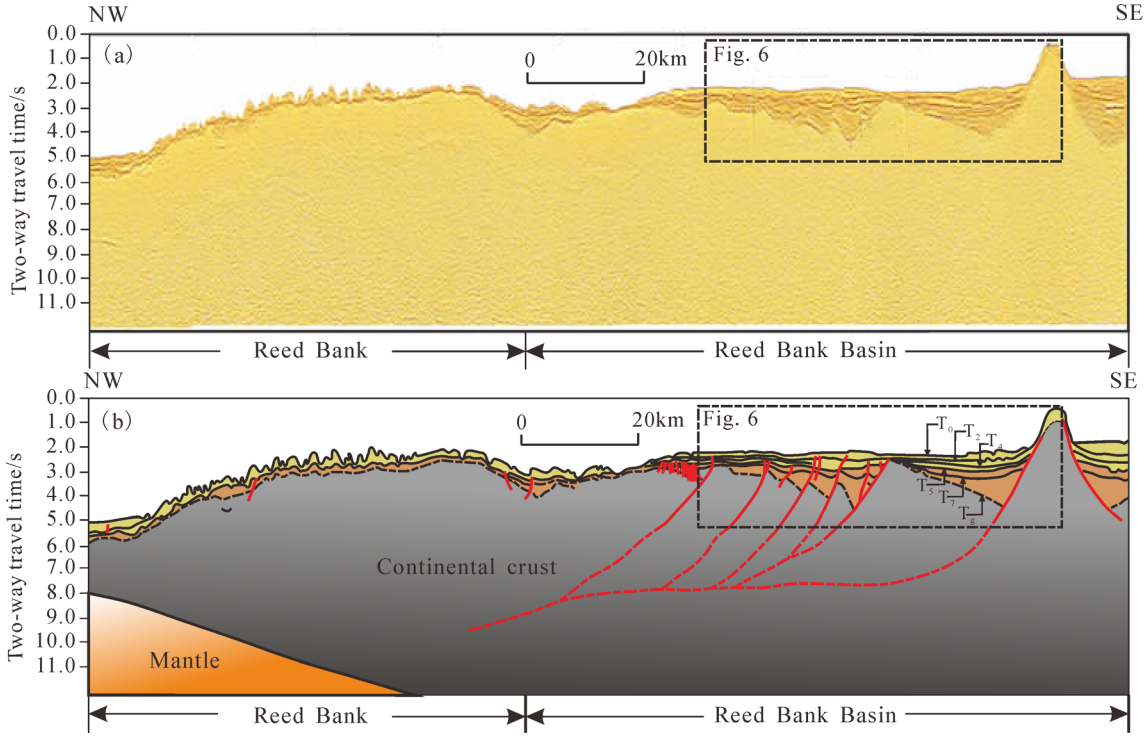

Fig. 4 Geological interpretations of multi-channel seismic profile NH973-2 in the Reed Bank area, South China Sea.

T_4 reflects the tectonic result of the collision between the Dangerous Grounds and Borneo areas, which halted the spreading in the SCS at about 15.5 Ma (Schlüter et al., 1996), or the Middle Miocene Unconformity (MMU) as described by Hutchison and Vijayan (2010). T_2 is another horizon in the post-drift sequence which is also the boundary between the Middle Miocene and Late Miocene, with an age of 10.5 Ma. T_0 is the interface of sea level.

3.3 Method of tectonic subsidence reconstruction and parameters

Tectonic subsidence in the basin generally refers to the subsidence caused by the deep tectonic movements in the basement (Ungerer et al., 1984). It is further described as the amount of subsidence that would have been experienced by the basement if it had only been air-loaded and is generally considered to have been caused by the inner tectonic force of the Earth; that is, the unloaded tectonic subsidence or air-loaded tectonic subsidence (Wu et al., 2003). Therefore, by removing the impact of the sedimentary compaction correction and global level changes, and understanding the uplift or subsidence of basement in the absence of a water-load correction, the quantification of basin subsidence becomes more difficult.

A 1-D unloaded (i.e., water and sediment unloaded) tectonic subsidence model was used in this study. Unloaded tectonic subsidence is the true tectonic subsidence without any load-induced isostatic subsidence, which makes the concept of tectonic subsidence clear and the analysis of dynamic mechanism easier. When considering the mechanism of the lithosphere subsidence and various controlling factors, the above mentioned method (Fig. 5) is based on the Airy isostasy to backstrip the present stratigraphy layer by layer and to obtain the true basement subsidence or lithospheric tectonic subsidence caused by the inner tectonic force of the earth (Zhao et al., 2013). In the process, reconstruction of tectonic subsidence is related to the tectonics, sediment compaction, and water-loaded, sedimentary basement level change and the palaeowater depth change. We have corrected these parameters respectively.

3.3.1 Sediment and water-loaded subsidence

According to the Airy isostasy model, when the space of the sedimentary basin is filled with the sediment, the weight of the sediment itself further submerges the basement leading to the formation of sediment loaded subsidence. The top and bottom boundary depth in different strata can be recovered by the porosity, and the amount of basement subsidence, which represents the depth of the oldest stratum, can also be obtained. On the basis of the water-loaded subsidence and the relationship between porosity and depth, we calculate the average density of the sediment and water in the strata. As a result, the burial depth and the amount of subsidence in each stratum can be determined.

The equation of subsidence proposed by Steckler and Watts (1978) is illustrated in Eq. (1). The loaded subsidence caused by sea level rise is taken into consideration (Fig. 5(c)), while alternatively, the water-loaded subsidence solely created by the water that filled in the accommodation space and was generated by tectonic subsidence, is disregarded. In light of the crustal isostatic principle, the increment of the water-load is the total weight of basement subsidence,excluding mantle material, and the total subsidence generated by the actual water-load, which is the sum of the base level and the increment of water-load (Eq. (2)). As such, the empty basin tectonic subsidence and unloaded tectonic subsidence rate for any

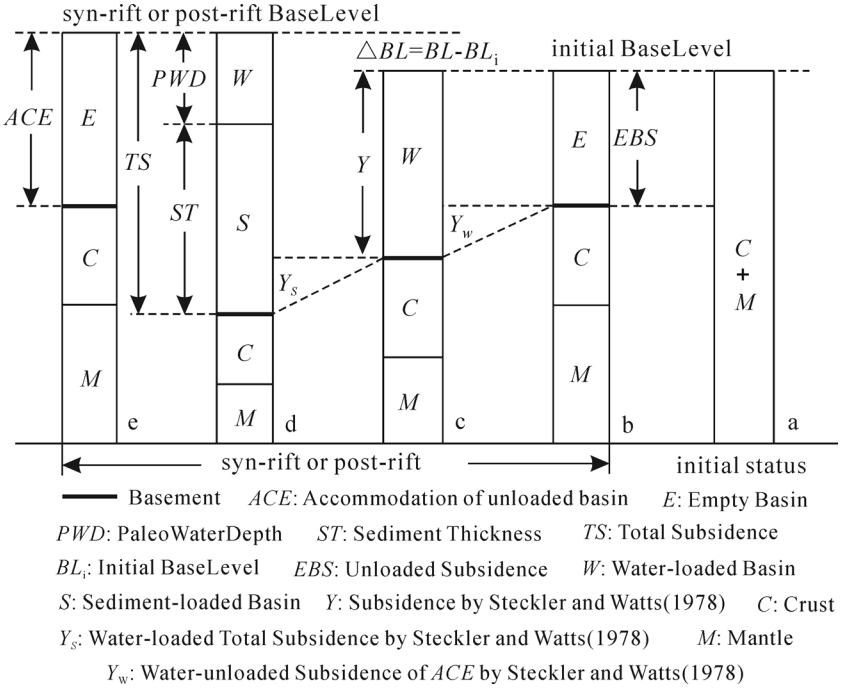

Fig. 5 The unloaded tectonic subsidence model (revised by Steckler and Watts, 1978 and Zhao et al., 2013).

two given time periods ($k \rightarrow n$, $k > n$) are given as follows (Eq. (3) and Eq. (4)) (Zhao et al., 2013).

$$\begin{aligned} Y &= TS - Y_w - BL \\ &= ST + (PWD + \Delta BL) - ST \times \frac{\rho_s - \rho_m}{\rho_m - \rho_w} - \Delta BL \times \frac{\rho_w}{\rho_m - \rho_w} \\ &= ST \times \frac{\rho_m - \rho_s}{\rho_m - \rho_w} + \Delta BL \times \frac{\rho_m}{\rho_m - \rho_w} + PWD, \end{aligned} \tag{1}$$

$$Y_s = Y_w + SL = Y \times \frac{\rho_w}{\rho_m} + \Delta BL \times \frac{\rho_w}{\rho_m - \rho_w}, \tag{2}$$

$$EBS = ST \times \frac{\rho_m - \rho_s}{\rho_m} + PWD \times \frac{\rho_m - \rho_w}{\rho_m} - \Delta BL, \tag{3}$$

$$\begin{aligned} EBSR_{k-n} &= (EBS_n - EBS_k)/(k-n) \\ &= \left[(ST_n - ST_k) \times \frac{\rho_m - \rho_s}{\rho_m} + (PWD_n - PWD_k) \right. \\ &\quad \left. \times \frac{\rho_m - \rho_w}{\rho_m} - (BL_n - BL_k)\right]/(k-n), \end{aligned} \tag{4}$$

where Y is the subsidence generated by tectonic driving force. As defined by Steckler and Watts (1978), Y_s is the total water-loaded subsidence and Y_w is the loaded subsidence caused by the water-filled accommodation space (ACE) generated by tectonic subsidence, EBS is the empty basin or unloaded tectonic subsidence, ST is sedimentary thickness, PWD is palaeowater depth, ΔBL is the change amount of base level, ρ_m, ρ_s, ρ_w is the average density of the mantle, sediment, and water respectively, and $EBSR$ is the empty basin or unloaded tectonic subsidence rate, and k and n represent two different periods ($k > n$).

3.3.2 Lithology

The sedimentary compaction is influenced by the lithology, overcompress, diagenesis, and other factors, wherein the lithology tends to play a leading role. There is a decrease in the porosity of sediment with an increase in overlying strata' thickness during the accumulation process. The density (ρ), porosity (Por), and compaction constant (CC) are determined by lithology and its statistical percentage (see detail parameters in Table 1) (revised by Zhao et al., 2010).

3.3.3 Palaeowater depth

The sedimentary thickness cannot represent the depth of subsidence when the palaeowater depth in the sedimentary basin is significant and the sedimentary interface remains below the water surface. The palaeowater depth can be determined by many sedimentary marks, such as the sediment distribution pattern, sedimentary structure, paleontology, paleoecology, and authigenic minerals, etc. (Clifton, 1988).

Table 1 The lithologic parameters of each layer in the Dangerous Grounds, and Reed Bank area (revised by Zhao et al., 2010)

	layer	Parameters		
		ρ/(kg·m^{-3})	Por	CC/mm^{-1}
Dangerous Grounds	T_2–T_0	26.93	0.60	0. 480
	T_4–T_2	26.94	0.59	0. 440
	T_5–T_4	26.91	0.59	0. 450
	T_7–T_5	27.07	0.62	0. 500
	T_g–T_7	26.76	0.56	0. 420
Reed Bank area	T_2–T_0	26.98	0.61	0. 500
	T_4–T_2	27.07	0.66	0. 615
	T_5–T_4	27.01	0.65	0. 590
	T_7–T_5	27.04	0.66	0. 620
	T_g–T_7	26.95	0.58	0. 430

The sediments show fluvial and swamp facies in the Mesozoic, and are composed of sandstone and shale, in addition to coal (Ding et al., 2015). Thus the water depth in the initial rifting stage (65 Ma) is assumed to be zero. Between the Paleocene and the Middle Oligocene (65–32 Ma) the sediments changed from abyssal facies characterized by gray and green–brown calcareous shales, to neritic facies, characterized by interbedded sandstone and mudstone, showing an overall decrease of water depth (from 500 to 100 m). During the drifting stage (32–23.8 Ma in the Reed Bank area, 32–19 Ma in the Dangerous Grounds), a well-developed carbonate platform indicated a palaeobathymetry of shallow water (less than 50 m). After 15.5 Ma, the water depth rapidly increased (where some part of the present-day bathymetry is greater than 3500 m). Although the eustatic sea-level fluctuation has less influence on backstripping, if compared to the variations of palaeo-bathymetry, the relative sea level change in the Cenozoic (Pang et al., 2007) has been incorporated in backstripping order to make the subsidence study integrity.

The determination of palaeowater depth in this study was generally based on the depositional systems, which were compiled by well data and seismic sequence studies. Therefore, the palaeowater depth was recovered by the sedimentary facies of basins in different periods and the paleontological in wells. Considering the sedimentary facies, foraminifera, and nannofossil in the southern SCS (Taylor and Hayes, 1980; Yang et al., 1996; Fan and Qian, 1998; Steuer et al., 2013), we used the interpolation method to reduce the error and to obtain the palaeowater depth.

3.3.4 Time-depth conversion

A time to depth conversion has been carried out to construct the cross sections used for subsidence analysis (Fig. 6). The time-velocity statics over the southern continental margin for reconstruction of subsidence history has been adopted according to Yan and Liu (2004) (Table 2).

4 Results

Calculation results of the tectonic subsidence rates and total amounts from each seismic profile are shown in Tables 3 and 4. Figures 7 and 8 demonstrate these results. An overview of the backstripped tectonic subsidence curves for all the selected artificial wells is shown in Fig. 9. Our study shows a total tectonic subsidence amount of 1225–2790 m along the NH973-1 across the Dangerous Grounds, and 1455–2015 m along the NH973-2 in the Reed Bank area. Both areas show different subsidence rates and the amounts in separated stages, i.e., the rate presents a regular promotion and demotion with the change of time. Generally the subsidence rate is higher inside graben/half-graben, but is smaller in the basement high between.

4.1 Dangerous Grounds (Seismic profile NH973-1)

The initial subsidence during the active extensional phase has been recognized from the Late Cretaceous (T_g, ~65 Ma) to the Early Oligocene (T_7, ~32Ma). During this stage, the tectonic subsidence rate is between 3.7~16 m/Ma, with an average rate of 6.1 m/Ma. Episodic rifting has been reported by previous studies (Zhou et al., 1995; Cullen, 2010), while in our study, a classification of extensional episodes has not been carried out, and the tectonic subsidence is simplified. Rapid subsidence has occurred since the Early Oligocene (T_7, ~32 Ma) with a subsidence rate between 43–111 m/Ma. The average

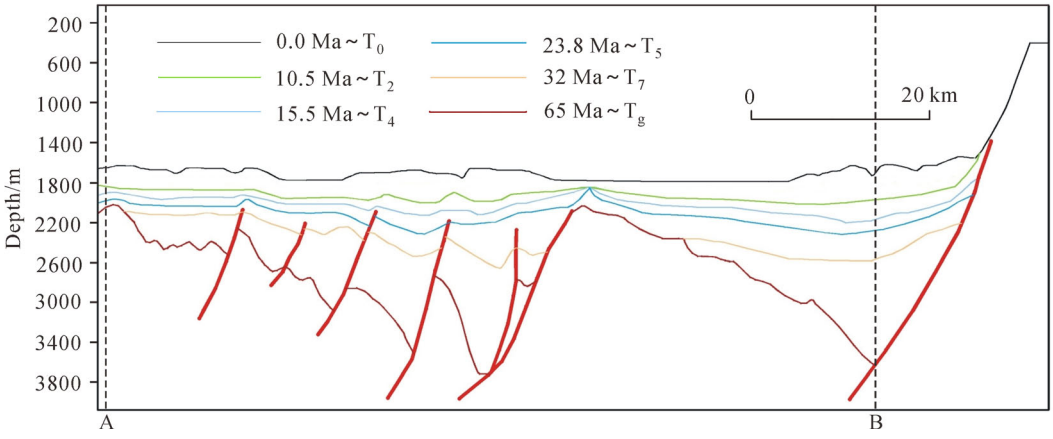

Fig. 6 Time-depth conversions of the NH973-2 multi-channel seismic section. A and B are the horizontal positions of tectonic subsidence calculation.

Table 2 Time-velocity statistics in southern continental margin of South China Sea (Yan and Liu, 2004)

TWT/s	Vn/(km·s^{-1})	TWT/s	Vn/(km·s^{-1})	TWT/s	Vn/(km·s^{-1})	TWT/s	Vn/(km·s^{-1})
0	1500	1.8	2244	3.6	2928	5.6	3414
0.2	1510	2.0	2330	3.8	2989	5.8	3453
0.4	1550	2.2	2418	4.0	3044	6.0	3492
0.5	1600	2.4	2494	4.1	3068	6.2	3529
0.6	1646	2.5	2532	4.3	3120	6.4	3578
0.8	1775	2.6	2577	4.5	3164	6.6	3621
1.0	1900	2.8	2642	4.6	3187	6.8	3662
1.2	1993	3.0	2720	4.8	3238	7.0	3700
1.4	2071	3.2	2800	5.0	3280		
1.5	2107	3.4	2871	5.2	3327		
1.6	2144	3.5	2891	5.4	3370		

Table 3 Calculation of tectonic subsidence rate

Profile	T_g-T_7 (65–32 Ma)		T_7-T_5 (32–23.8 Ma for NH973-2; 32–19 Ma for NH973-1)		T_5-T_4 (23.8–15.5 Ma for NH973-2; 19–15.5 Ma for NH973-1)		T_4-T_2 (15.5–10.5 Ma)		T_2-T_0 (10.5–0 Ma)	
	Ran	Ave	Ran	Ave	Ran	Ave	Ran	Ave	Ran	Ave
NH973-1	3.7–16	6.1	43–111	72	–33–130	18.9	76–147	109	33–85.6	53.4
NH973-2	7.7–23	12.9	–9.7–7.6	–4.3	62.5–77	69.9	98–105	101.2	48.8–58	55.7

* where, Ran represent the range of values, Ave represent the average value.

Table 4 Calculation of tectonic subsidence amount

Profile	T_g-T_7 (65–32 Ma)		T_7-T_5 (32–23.8 Ma for NH973-2; 32–19 Ma for NH973-1)		T_5-T_4 (23.8–15.5 Ma for NH973-2; 19–15.5 Ma for NH973-1)		T_4-T_2 (15–10.5 Ma)		T_2-T_0 (10.5–0 Ma)	
	Ran	Ave	Ran	Ave	Ran	Ave	Ran	Ave	Ran	Ave
NH973-1	150–640	242	364–946	609	–49–276	32	344–659	491	348–910	562
NH973-2	270–795	453	–107–84	–48	231–285	258	468–502	485	550–602	578

* where, Ran represent the range of values, Ave represent the average value.

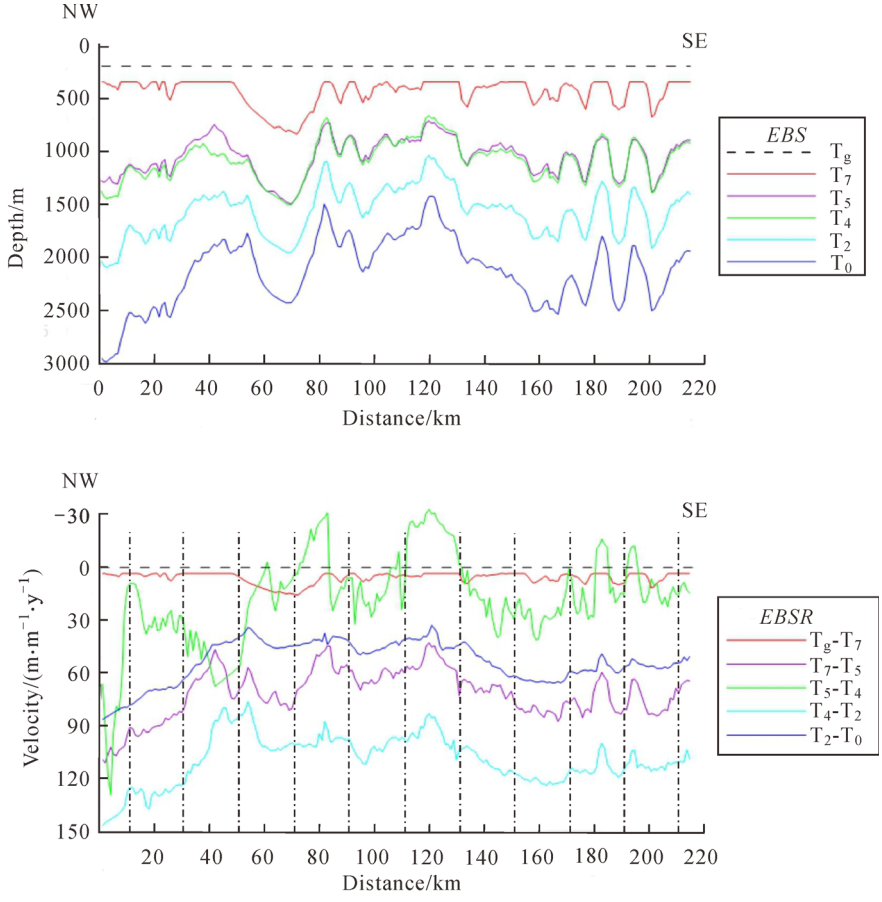

Fig. 7 The tectonic subsidence rate and total amount of the NH973-1 multi-channel seismic profiles in the Dangerous Grounds, Southern South China Sea. *EBS* is Empty Basin tectonic Subsidence, *EBSR* is Empty Basin tectonic Subsidence Rate.

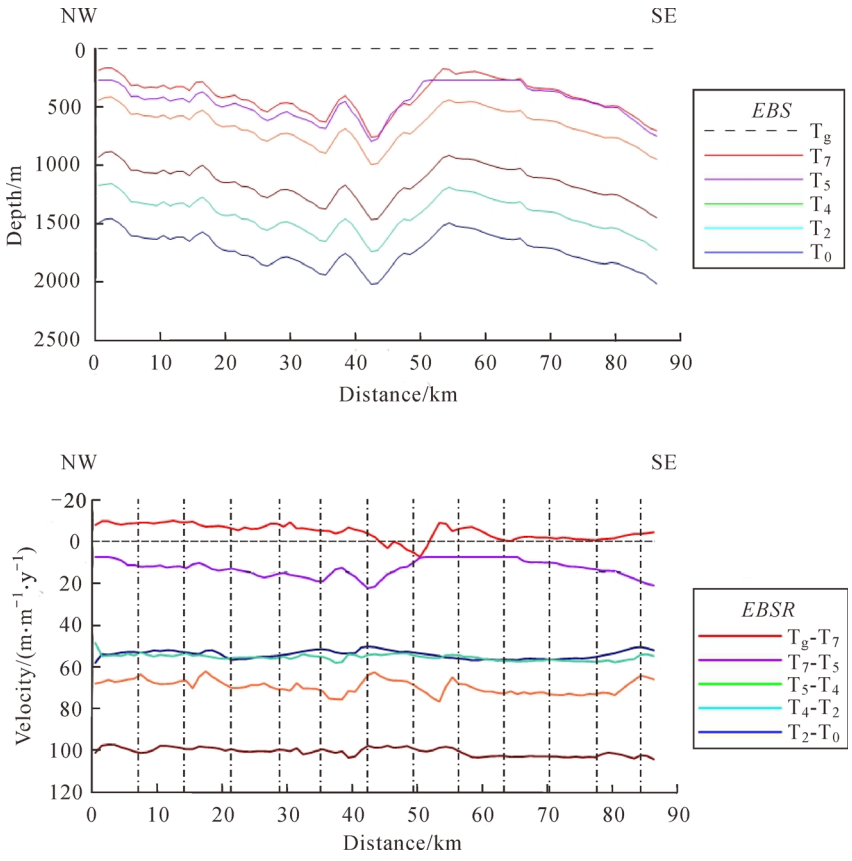

Fig. 8 The tectonic subsidence rate and total amount of the NH973-2 multi-channel seismic profiles in the Reed Bank area, Southern South China Sea. EBS is Empty Basin tectonic Subsidence, EBSR is Empty Basin tectonic Subsidence Rate.

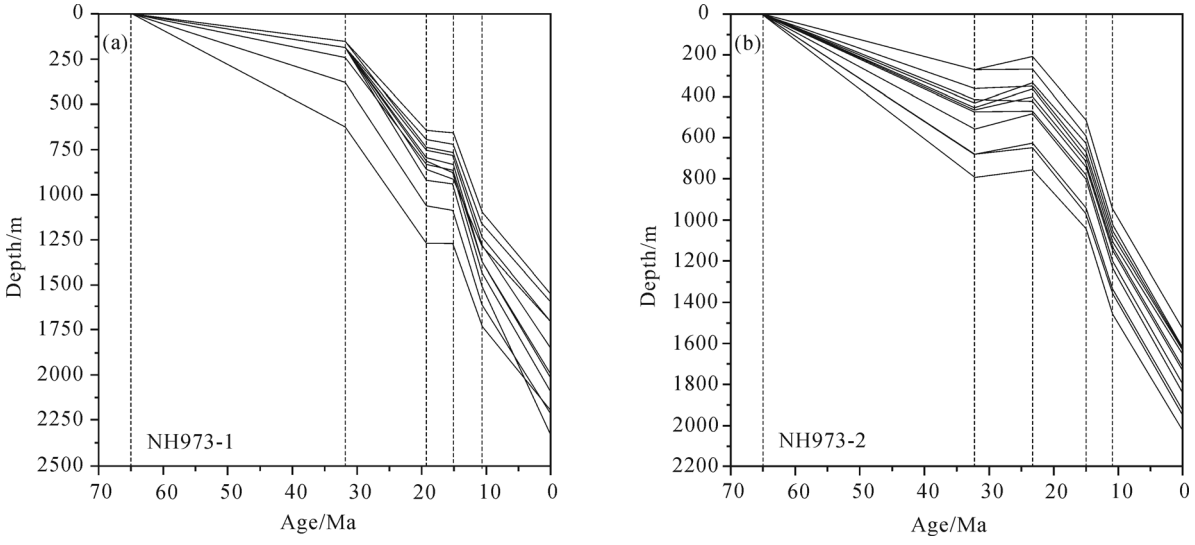

Fig. 9 An overview of the backstripped tectonic subsidence curves. (a) The unloaded tectonic subsidence curve in the Dangerous Grounds area; (b) the unloaded tectonic subsidence curve in the Reed Bank area.

rate is 72 m/Ma. In the late Oligocene (T_5, ~19 Ma), the subsidence rate reduced sharply to between –33–130 m/Ma. This slow subsidence stage lasted nearly 4 m.y. until a rate increase was observed in the Middle Miocene (T_4, ~15.5 Ma), corresponding to the drifting of the SCS. This accelerated subsidence stage since the Middle

Miocene has a subsidence rate of 76–147 m/Ma, which is common in the continental margin of the SCS (Clift and Lin, 2001; Zhao et al., 2013; Chen, 2014).

4.2 Reed Bank area (Seismic profile NH973-2)

Tectonic subsidence in the Reed Bank area decreased between the late Cretaceous (T_g, ~65 Ma) and the Early Oligocene (T_7, ~32Ma), similar to the trends observed in the Dangerous Grounds area. The subsidence rate was between 7.7 and 23 m/Ma, with an average of 12.9 m/Ma. However, the rate reduced sharply in the Early Oligocene (T_7, ~32 Ma) with an average of –4.3 m/Ma. This slow subsidence rate lasted for more than 10 m.y. An accelerated subsidence occurred after the Early Miocene and continued until the Late Miocene. The subsidence rate was between 98 and 105 m/Ma, averaging 101.2 m/Ma. This indicates a quick thermal subsidence during the post-spreading stage and a sharp change of sedimentary environment. In the Late Miocene, the subsidence rate smoothed from the earlier stage, but remained relatively high, between 48.8–58 m/Ma, to the present.

5 Discussion

5.1 Why the subsidence rate delayed?

The subsidence of rifted continental margins is explained by the mechanical and isostatic response to the lithospheric stretching (McKenzie, 1978). Moreover, generally rapid thermal subsidence would occur after the continental break-up when an initial seafloor spreading is driven by cooling and thickening of the asthenosphere. However, our analysis results of tectonic subsidence show that neither the Reed Bank nor the Dangerous Grounds entered the rapid subsidence stage after the onset of seafloor spreading, but instead experienced an uplift and erosion period. According to the results of tectonic subsidence, the subsidence hiatus phenomenon can be recognized between 19–15.5 Ma in the Dangerous Grounds (Fig. 9(a)). Similar subsidence rate delay could also be discovered in the Reed Bank area which mutated and gradually slowed between 32 and 23.8 Ma (Fig. 9(b)). The rapid subsidence period only occurred after the cessation of seafloor spreading. Considering the data from carbonate platform and its drilling result in the Neogene, this phenomenon is similar to the large scale development of the carbonate platform stage ($T_7 - T_4$, 32–15.5Ma) which corresponds to a greatly reduced tectonic subsidence rate (Ding et al., 2015; Fang et al., 2015). As such, the cause for the temporary subsidence delay in the southern continental margin of SCS becomes a key issue in our study.

This lack of tectonic subsidence may be the result of a number of possible processes. Since the thermal subsidence is driven by the lithospheric thickening (Sandiford et al., 1998), we suggest that the slow subsidence after break-up indicates a slow lithospheric growth. The normal subsidence and lithospheric thickening does not occur until after 23.8 Ma in the Reed bank area, and 15.5 Ma in the Dangerous Grounds area. Reston (2009) suggested that the effect of mantle serpentinization during rifting, or the addition of any igneous material at sub-crustal level, could result in permanent uplift. However, our results show a temporary rather than a permanent subsidence rate. Thus we may exclude this possibility. Franke et al. (2011) argued another hypothesis that the ongoing westward rifting in the SWSB might have prevented the region from quick subsidence. Although we can't exclude this mechanism, we prefer the opinion that the secondary mantle convection (first or major mantle convection occurred in the oceanic basin) may be a more reasonable process. The secondary mantle convection in the mantle beneath a rift in the continental margin may have eroded the lithosphere and caused the very slow lithospheric growth after the initial sea-floor spreading.

Numerical experiments have proved that as the major mantle convection occurred below the oceanic crust, a variation in lithospheric thickness of the continental margin will cause lateral temperature gradients, and thus induce secondary convection (Buck, 1986; Faccenna and Becker, 2010), or edge-driven convection (King and Anderson, 1998). This convection beneath the passive rifts will result in the thinning of the adjacent lithosphere, controlling the uplift of the rift shoulders, as well as the decrease of the tectonic subsidence in the middle of the rift basin. This geodynamic model has been successfully applied in many cases, such as the rifted margin of Pakistan (Clavès et al., 2008), or the Atlantic margin (Buck, 1986; Van Wijk et al., 2008, 2010).

The crustal structure in the Reed Bank area obtained by the wide-angle reflection/refraction seismic experiments shows that the crustal thickness in the Bank is about 21 km, and yet the crustal thickness at the Reed Bank basin periphery is only 12 km, indicating that the Moho depth gap is about 9 km (Ruan et al., 2011). In the Dangerous Grounds area, the Moho depths also had a high frequency of fluctuation, ranging between 17–26 km (Qin et al., 2011; Pichot et al., 2014). Such a gap in the lithospheric thickness was likely to cause steep vertical temperature contrasts, and then induced a secondary mantle convection, which may be the reason for the decrease of the tectonic subsidence rate in the study area during break-up. After the cessation of seafloor spreading, the mantle convection beneath the oceanic crust disappeared, and the secondary mantle convection under the continental margin in southern SCS also stopped. The whole area entered the rapid subsidence stage.

5.2 Why the delayed stage changes?

It is obvious that the stage with delayed subsidence rate

differed between areas. In the Reed Bank area, this stage was between 32–23.8 Ma, while in the Dangerous Grounds it was much later (between 19–15.5 Ma). We believe the propagated rifting in the SCS determined the changes of delayed-subsidence-rate stage.

Neotectonic and sedimentary variation in the continental margin have been well studied by previous scientists (Shipboard Scientific Party, 2000; Yao et al., 2012; Ding et al., 2013; Franke et al., 2014; Savva et al., 2014). Inhomogenous tectono-sedimentary features can also be observed in the oceanic basin. Geological observations in the basin of the SWSB suggest that the NE section is dominated by normal oceanic crust formed in a steady state and spreading with a high magma budget, indicated by the reasonably flat oceanic basement, increasing sedimentary thickness from the middle to both sides, and active post-drift magmatic activities (Huchon et al., 2001; Li et al., 2012; Ding et al., 2015). Studies of both the continental margin and the oceanic basin of the SWSB indicate a number of differences in the tectono-sedimentary fabric from the northeast to the southwest. 1) Intense continental rifting occurred in the Reed Bank area, which reduced to the southwest. 2) The time of cessation of rifting, which resulted from the onset of the opening of the SWSB, became younger from the Reed Bank area to the west of the Dangerous Grounds. 3) An increased magma budget in the NE section of the oceanic basin. All these features suggest that: 1) the rifting and seafloor spreading should have started in the northeastern area and propagated to the southwest, and 2) the northeastern area experienced longer seafloor spreading, implied by the typically wider oceanic basin, whereas the relatively short spreading history in the southwestern area formed a narrow oceanic basin with remarkable continental rifting features.

The delayed stage in the Reed Bank area, resulting from the seafloor spreading in the ESB, was initiated much earlier. Alternatively, the delayed stage in the Dangerous Grounds area didn't begin until after the opening of the SWSB. We should note that the delayed tectonic subsidence stopped after 23.8 Ma while the seafloor spreading was still ongoing in the ESB and the SWSB. The ESB has experienced a longer spreading history and had already become a wide oceanic basin before the opening of the SWSB. After 23.8 Ma, the Reed Bank area was far away from the spreading center, which might have reduced the possibility of the formation of a second-convection. However, during the Early Miocene, the Dangerous Grounds area was still close to the spreading center of the SWSB. This might explain why the tectonics subsidence rate increased in the Reed Bank area as the seafloor spreading was taking place in the Early Miocene.

6 Conclusions

1) The Cenozoic tectonic subsidence can be roughly divided into three stages with variable subsidence rate in the southern continental margin. The first rapid-subsidence-rate stage occurred during 65 to 19 Ma in the Dangerous Grounds area and 65 to 23.8 Ma in the Reed Bank area, while the delayed-subsidence-rate stage can be recognized during 19 to 15.5 in the Dangerous Grounds and 23.8 to 15.5 Ma in the Reed Bank area followed by the second rapid-subsidence-rate stage.

2) As the major mantle convection occurred below the oceanic crust, a variation in lithospheric thickness was likely to cause steep vertical temperature contrasts, which then induced a secondary mantle convection. We believe this secondary convection resulted in the period of minimal lithospheric growth, and may be the reason for the delayed tectonic subsidence rate during the seafloor spreading in the southern continental margin.

3) The stage with delayed subsidence rate differed along strikes. In the Reed Bank area, this stage is between 32–23.8 Ma, while in the Dangerous Grounds, it was much later (between 23.8–15.5 Ma). We believe the propagated rifting in the SCS determined the changes of the delayed-subsidence-rate stage.

Acknowledgements We want to thank the anonymous reviewers for their helpful comments. This paper benefits from early discussions with Peter D Clift from State Louisiana Univeristy. This work was financially supported by the National Natural Science Foundation of China (No. 41376066), the National Program on Global Change and Air-Sea Interaction, SOA (No. GASI-GEOGE-01), MOST of China (No. 2016YFC0600402), and Continental Shelf Drilling Project (No. GZH201100202).

References

Aurelio M A, Peña R E, Taguibao K J L (2012). Sculpting the Philippine archipelagosince the cretaceous through rifting, oceanic spreading, subduction, obduction,collision and strike-slip faulting: contribution to IGMA5000. J Asian Earth Sci, 72(4): 102–107

Barckhausen U, Engels M, Franke D, Ladage S, Pubellierb M (2014). Evolution of the South China Sea: revised ages for breakup and seafloor spreading. Mar Pet Geol, 58: 599–611

Barckhausen U, Roeser H A (2004). Seafloor spreading anomalies in the South China Sea revisited. Continent-ocean interactions within East Asian marginal seas, 121–125

Briais A, Patriat P, Tapponnier P (1993). Updated interpretation of magnetic anomalies and seafloor spreading stages in the South China Sea: implications for the Tertiary tectonics of Southeast Asia. Journal of Geophysical Research: Solid Earth (1978–2012), 98(B4): 6299–6328

Buck W R (1986). Small-scale convection induced by passive rifting: the cause for uplift of rift shoulders. Earth Planet Sci Lett, 77(3-4): 362–372

Chen L (2014). Stretching factor estimation for the long-duration and multi-stage continental extensional tectonics: application to the Baiyun Sag in the northern margin of the South China Sea. Tectonophysics, 611: 167–180

Clavès G, Clift P D, Inam A (2008). Anomalous Subsidence on Rifted

Volcanic Margin of Pakistan: No Influence from Deccan Plume. Earth Planet Sci Lett, 272(1–2): 231–239

Clift P, Lee G H, Nguyan A D, Barckhausen U, Long H V, Sun Z (2008). Seismic reflection evidence for a dangerous grounds miniplate: no extrusion origin for the South China Sea. Tectonics, 27, TC3008

Clift P, Lin J (2001). Preferential mantle lithospheric extension under the South China margin. Mar Pet Geol, 18(8): 929–945

Clifton H E (1988). Sedimentologic approaches to paleobathymetry, with applications to the Merced Formation of central California. Palaios, 3(5): 507–522

Cullen A B (2010). Transverse segmentation of the Baram-Balabac Basin, NW Borneo: refining the model of Borneo's tectonic evolution. Petrol Geosci, 16(1): 3–29

Ding W W, Franke D, Li J B, Steuer S (2013). Seismic stratigraphy and tectonic structure from a composite multi-channel seismic profile across the entire Dangerous Grounds, South China Sea. Tectonophysics, 582: 162–176

Ding W W, Li J B, Dong C Z, Fang Y X (2015). Oligocene-Miocene carbonates in the Reed Bank area, South China Sea, and their tectono-sedimentary evolution. Mar Geophys Res, 36(2-3): 149–165

Ding W W, Li J B, Li M B (2011). Seismic stratigraphy, tectonic structure and extension model across the Reed Bank Basin in the South China Sea: evidence from NH973-2 multi-channel seismic profile. Earth Science-Journal of China University of Geosciences, 36(5): 895–904 (in Chinese)

Expedition 349 Scientists (2014). South China Sea tectonics: opening of the South China Sea and its implications for southeast Asian tectonics, climates, and deep mantle processes since the late Mesozoic. International Ocean Discovery Program Preliminary Report, 349

Faccenna C, Becker T W (2010). Shaping Mobile Belts by Small-scale Convection. Nature, 465(7298): 602–605

Fan K Y, Qian G H (1998). The Cenozoic stratigraphic division and correlation in Nansha Waters. China Offshore Oil And Gas (Geology), 12(6): 370–376 (in Chinese)

Fang P G, Ding W W, Fang Y X, Zhao Z X (2015). Development of Carbonate Platform and Its Response to Cenozoic Subsidence in Reed Bank Area, the South China Sea. Earth Science—Journal of China University of Geoscience, 40(12) :2052–2066 (in Chinese)

Franke D (2013). Rifting, lithosphere breakup and volcanism: Comparison of magma-poor and volcanic rifted margins. Mar Pet Geol, 54(3): 63–87

Franke D, Barckhausen U, Baristeas N, Engels M, Ladage S, Lutz R, Montano J, Pellejera N, Ramos E G, Schnabel M (2011). The continent-ocean transition at the southeastern margin of the South China Sea. Mar Pet Geol, 28(6): 1187–1204

Franke D, Barckhausen U, Heyde I, Tingay M, Ramli N (2008). Seismic images of a collision zone offshore NW Sabah/Borneo. Mar Pet Geol, 25(7): 606–624

Franke D, Savva D, Pubellier M, Steuer S, Mouly B, Auxietre J L, Meresse F, Chamot-Rooke N (2014). The final rifting evolution in the South China Sea. Mar Pet Geol, 58: 704–720

Hall R (2002). Cenozoic geological and plate tectonic evolution of SE Asia and the SW Pacific: computer-based reconstructions, model and animations. J Asian Earth Sci, 20(4): 353–431

Hall R, Clements B, Smyth H R (2009). Sundaland: basement character, structure and plate tectonic development. In: Proceedings, Indonesian Petroleum Association Thirty-Third Annual Convention and Exhibition, May 2009

Hall R, van Hattum M W A, Spakman W (2008). Impact of India–Asia collision on SE Asia: the record in Borneo. Tectonophysics, 451(1): 366–389

Hayes D E, Nissen S S (2005). The South China Sea margins: implications for rifting contrasts. Earth Planet Sci Lett, 237(3-4): 601–616

Hinz K, Schlüter H U (1985). Geology of the dangerous grounds, South China Sea, and the continental margin off southwest Palawan: results of SONNE Cruises SO-23 and SO-27. Energy, 10(3): 297–315

Honza E (1995). Spreading mode of backarc basins in the western Pacific. Tectonophysics, 251(1–4): 139–152

Honza E, Fujioka K (2004). Formation of arcs and backarc basins inferred from the tectonic evolution of Southeast Asia since the Late Cretaceous. Tectonophysics, 384(1-4): 23–53

Huchon P, Nguyen T N H, Chamot-Rooke N (2001). Propagation of continental break-up in the south-western South China Sea. In: Wilson R C L, Whitmarsh R B, Taylor B, Froitzheim N, eds. Nonvolcanic rifting of continental margins: a comparison of evidence from land and sea. London: Special Publication Geological Society, 187: 31–50

Hutchison C S (2004). Marginal basin evolution: the southern South China Sea. Mar Pet Geol, 21(9): 1129–1148

Hutchison C S, Bergman S C, Swauger D A, Graves J E (2000). A Miocene collisional belt in north Borneo: uplift mechanism and isostatic adjustment quantified by thermochronology. J Geol Soc London, 157(4): 783–793

Hutchison C S, Vijayan V (2010). What are the Spratly Islands? J Asian Earth Sci, 39(5): 371–385

King S D, Anderson D L (1998). Edge-driven convection. Earth Planet Sci Lett, 160(3-4): 289–296

Kudrass H R, Wiedicke M, Cepek P, Kreuzer H, Müller P (1986). Mesozoic and Cainozoic rocks dredged from the South China Sea (Reed Bank area) and Sulu Sea and their significance for plate-tectonic reconstructions. Mar Pet Geol, 3(1): 19–30

Lee T Y, Lawver L A (1995). Cenozoic plate reconstruction of Southeast Asia. Tectonophysics, 251(1-4): 85–138

Li C, Song T (2012). Magnetic recording of the Cenozoic oceanic crustal accretion and evolution of the South China Sea basin. Chin Sci Bull, 57(24): 3165–3181

Li C F, Xu X, Lin J, Sun Z, Zhu J, Yao Y J, Zhao X X, Liu Q S, Kulhanek D K, Wang J, Song T R, Zhao J F, Qiu N, Guan Y, Zhou Z, Williams T, Bao R, Briais A, Brown E A, Chen Y, Clift P D, Colwell F S, Dadd K A, Ding W, Almeida I H, Huang X L, Hyun S, Jiang T, Koppers A A P, Li Q, Liu C, Liu Z, Nagai R H, Peleo-Alampay A, Su X, Tejada M L G, Trinh H S, Yeh Y C, Zhang C, Zhang F, Zhang G L (2014b). Ages and magnetic structures of the South China Sea constrained by deep tow magnetic surveys and IODP Expedition 349. Geochem Geophys Geosyst, 15(12): 4958–4983

Li J B (2011). Dynamics of the Continental Margins in South China Sea: Scientific Experiments and Research Progresses. Chin J Geophys, 54 (6): 883–893 (in Chinese)

Li S Z, Suo Y H, Liu X, Liming Dai S Y, Zhao S J (2012). Basic structural pattern and tectonic models of the South China Sea:

problems, advances and controversies. Marine Geology & Quaternary Geology, 32(6): 35–53 (in Chinese)

Li S, Zhao S, Liu X, Suo Y, Cao H, Dai L, Guo L, Liu B, Yu S, Zhang G (2014a). Processes of Ocean Continent Transition and Coupling. Periodical of Ocean University of China, 44(10): 113–133 (in Chinese)

Li X H, Li Z X, Li W X, Liu Y, Yuan C, Wei G J, Qi C S (2007). U–Pb zircon, geochemical and Sr–Nd–Hf isotopic constraints on age and origin of Jurassic I- and A-type granites from central Guangdong, SE China: A major igneous event in response to foundering of a subducted flat-slab? Lithos, 96(1-2): 186–204

McKenzie D (1978). Some remarks on the development of sedimentary basins. Earth Planet Sci Lett, 40(1): 25–32

Pang X, Chen C M, Peng D J, Zhu M, Shu Y, He M, Shen J, Liu B J (2007). Sequence stratigraphy of Pearl River Deep-water Fan System in the South China Sea. Earth Sci Front, 14(1): 220–229 (in Chinese)

Pichot T, Delescluse M, Chamot-Rooke N, Pubellier M, Qiu Y, Meresse F, Sun G, Savva D, Wong K P, Watremez L, Auxiètre J L (2014). Deep crustal structure of the conjugate margins of the SW South China Sea from wide-angle refraction seismic data. Mar Pet Geol, 58: 627–643

Qin J X, Hao T Y, Xu Y, Song H, Lu C C, Hu W J (2011). The distribution characteristics and the relationship between the tectonic units of the Moho Depth in South China Sea and Adjacent Areas. Chin J Geophys, 54(12): 3171–3183 (in Chinese)

Reston T J (2009). The Extension Discrepancy and Syn-Rift Subsidence Deficit at Rifted Margins. Petrol Geosci, 15(3): 217–237

Ru K, Pigott J D (1986). Episodic rifting and subsidence in the South China Sea. AAPG Bulletin, September, 70: 1136–1155

Ruan A G, Niu X W, Qiu X L, Li J B, Wu Z L, Zhao M H (2011). A wide angle ocean bottom seismometer profile across Liyue Bank, the southern margin of South China Sea. Chin J Geophys, 54(12): 3139–3149 (in Chinses)

Sandiford M, Hand M, Mclaren S (1998). High geothermal gradient metamorphism during thermal subsidence. Earth Planet Sci Lett, 163 (1-4): 149–165

Savva D, Pubellier M, Franke D, Chamot-Rooke N, Meresse F, Steuer S, Auxietre J L (2014). Different expressions of rifting on the South China Sea margins. Mar Pet Geol, 58: 579–598

Schlüter H U, Hinz K, Block M (1996). Tectono-stratigraphic terranes and detachment faulting of the South China Sea and Sulu Sea. Mar Geol, 130(1-2): 39–78

Shipboard Scientific Party (2000) Leg 184 summary: exploring the Asian Monsoon through drilling in the South China Sea. In: Wang P, Prell W, Blum P, eds. Proc. ODP, Initial results. IODP, College Station, TX, 1–77

Song T, Li C F (2015). Rifting to drifting transition of the Southwest Subbasin of the South China Sea. Mar Geophys Res, 36(2-3): 167-185.

Steckler M S, Watts A B (1978). Subsidence of the Atlantic-type continental margin off New York. Earth Planet Sci Lett, 41(1): 1–13

Steuer S, Franke D, Meresse F, Savvab D, Pubellierb M, Auxietrec J L (2013). Oligocene–Miocene carbonates and their role for constraining the rifting and collision history of the Dangerous Gounds, South China Sea. Mar Pet Geol, 76: 412–427

Sun Z, Zhao Z X, Zhou D, Yang S K, Lin H M (2011). The stratigraphy and the sequence achitecture of the basins in Nansha Region. Earth Science-Journal of China University of Geosciences, 36(5): 798–806 (in Chinese)

Sun Z, Zhong Z, Keep M, Zhou D, Cai D S, Li X H, Wu S M, Jiang J Q (2009). 3D analogue modeling of the South China Sea: a discussion on breakup pattern. J Asian Earth Sci, 34(4): 544–556

Taylor B, Hayes D E (1980). The tectonic evolution of the South China Basin. The tectonic and geologic evolution of Southeast Asian seas and islands, 89–104

Taylor B, Hayes D E (1983). Origin and history of the South China Sea basin. The Tectonic and Geologic Evolution of Southeast Asian Seas and Islands: Part 2, 23–56

Tong D J, Ren J Y, Lei C, Yang H Z, Yin X Y (2009). Lithosphere stretching model of deep water in Qiongdongnan Basin, northern continental margin of South China Sea and controlling of the post-rift subsidence. Earth Sci, 34(6): 963–974 (in Chinese)

Ungerer P, Bessis F, Chenet P Y, Durand B, Nogaret E, Chiarelli A, Oudin J L, Perrin J F (1984). Geological and geochemical models in oil exploration; principles and practical examples. In Demaison G, Murris R J, eds. Petroleum Geochemistry and Basin Evaluation: AAPG Memoir, 35: 53–77

Van Wijk J W, Baldridge W S, van Hunen J, Goes S, Aster R C, Coblentz D (2010). Small-scale Convection at the Edge of the Colorado Plateau: Implications for Topography, Magmatism, and Evolution of Proterozic Lithosphere. Geology, 38(7): 611–614

Van Wijk J W, Van Hunen J, Goes S (2008). Small-scale Convection during Continental Rifting: Evidence from the Rio Grande Rift. Geology, 36(7): 575–578

Wu N Y, Zeng W J, Song H B, Zhou Z Y, Du D L, Wan L (2003). Tectonic subsidence of the South China Sea. Marine Geology & Quaternary Geology, 23(1): 55–65 (in Chinese)

Xie H, Zhou D, Li Y, Pang X, Li P C, Chen G H, Li F C, Cao J H (2014). Cenozoic tectonic subsidence in deepwater sags in the Pearl River Mouth Basin, northern South China Sea. Tectonophysics, 615: 182–198

Yan P, Liu H (2004). Tectonic-stratigraphic division and blind fold structures in Nansha Waters, South China Sea. J Asian Earth Sci, 24 (3): 337–348

Yang M Z, Wu J M, Yang R, Duan W W (1996). Stratigraphic division and nomenclature of the southwestern Nansha sea area. Geol. Res. South China Sea, 8: 37–46 (in Chinese)

Yao B C (1996). Tectonic evolution of the south china sea in Cenozoic. Marine Geology & Quaternary Geology, 16(2): 1–12 (in Chinese)

Yao Y J, Liu H L, Yang C P, Han B, Tian J J, Yin Z X, Gong J L, Xu Q Y (2012). Characteristics and evolution of Cenozoic sediments in the Liyue Basin, SE South China Sea. J Asian Earth Sci, 60: 114–129

Yeh Y, Sibuet J, Hsu S, Liu C (2010). Tectonic evolution of the Northeastern South China Sea from seismic interpretation. J Geophys Res Solid Earth, 115, B060103

Yumul G P Jr, Dimalanta C B, Maglambayan V B, Marquez E J (2008). Tectonic setting of a composite terrane: a review of the Philippine island arc system. Geosci J, 12(1): 7–17

Yumul G P Jr, Dimalanta C B, Tamayo R A Jr, Maury R C (2003). Collision, subduction and accretion events in the Philippines: a synthesis. Isl Arc, 12(2): 77–91

Zhao Z X, Sun Z, Chen G H (2011). Cenozoic structural characteristics and subsidence evolution in Nansha. Earth Science-Journal of China University of Geosciences, 36(5): 815–822 (in Chinese)

Zhao Z X, Sun Z, Wang Z, Sun Z P, Liu J B, Wang Z W, Sun L T (2013). The dynamic mechanism of post-rift accelerated subsidence in Qiongdongnan Basin, northern South China Sea. Mar Geophys Res, 34(3-4): 295–308

Zhao Z X, Zhou D, Liao J, He M, Guo X Y, Zhang Y F, Xu Z Y (2010). Lithospheric Stretching Modeling of the Continental Shelf in the Pearl River Mouth Basin and Analysis of Post-Breakup Subsidence. Acta Geol Sin, 84(8): 1135–1145 (in Chinese)

Zhou D, Ru K, Chen H (1995). Kinematics of Cenozoic extension on the South China Sea continental margin and its implications for the tectonic evolution of the region. Tectonophysics, 251(1): 161–177

Zhou D, Sun Z, Chen H, Xu H H, Wang W Y, Pang X, Cai D S, Hu D K (2008). Mesozoic paleogeography and tectonic evolution of South China Sea and adjacent areas in the context of Tethyan and Paleo-Pacific interconnections. Isl Arc, 17(2): 186–207

Zhu D, Larin K V, Luo Q, Tuchin V V (2013). Recent progress in tissue optical clearing. Laser Photonics Rev, 7(5): 732–757